JURNAL LOCUS: Penelitian & Pengabdian
Volume 4 No. 12 December 2025
E-ISSN 2829-7334| P-ISSN 2829-5439
Hompage: https://locus.rivierapublishing.id/index.php/jl

# Numerical Study for Predicting the Initial Flash Point in Geothermal Wellbore: An Euler-Cauchy Method Approach

**Subhan Hasisi*, Khasani, Fauzun**
Universitas Gadjah Mada, Indonesia
Email: subhanhasisi@mail.ugm.ac.id*, khasani@ugm.ac.id, fauzun71@ugm.ac.id

***Abstract:***
*The precise forecasting of the initial flash point in geothermal wellbores is a crucial determinant for characterizing two-phase flow dynamics, the initiation of scaling, and overall well productivity. Despite the prevalence of considerable dissolved $CO_2$ in numerous geothermal reservoirs, prevailing wellbore simulators frequently overlook the thermodynamic interactions between $CO_2$ and $H_2O$. This study introduces a one-dimensional Euler-Cauchy numerical model founded on the conservation laws of mass, momentum, and energy, which is coupled with a thermodynamic framework that explicitly accounts for $CO_2$. This framework incorporates $CO_2$ solubility, vapor-liquid equilibrium, and the corresponding variations in mixture properties. A parametric analysis was conducted across $CO_2$ mass fractions of 0.00% to 1.00%. The simulations reveal that increased $CO_2$ concentrations displace the flash point to greater depths within the wellbore: 1409.5 m, 1312 m, 1233 m, 1174 m, and 1134 m for 1.00%, 0.75%, 0.50%, 0.25%, and 0.00% $CO_2$, respectively. These results underscore the significant impact of non-condensable gases on geothermal well performance and provide critical insights for managing scale formation, mitigating corrosion, and optimizing operations.*

***Keywords***: *geothermal wellbore, flash point prediction, $CO_2$, Euler-Cauchy*

*Corresponding*: Subhan Hasisi
E-mail: subhanhasisi@mail.ugm.ac.id

## INTRODUCTION

Geothermal energy extraction fundamentally relies on the production of high-enthalpy fluids from subterranean reservoirs. The ascent of these fluids through the production wellbore is characterized by a continuous pressure decrease, which induces a critical thermodynamic transition (Ibrahim, 2021; Liu, Bin Xiao, Zhuang, Li, & Li, 2025). The depth at which the fluid pressure falls below its saturation pressure marks the first flash point, initiating a shift to two-phase flow (Guo et al., 2022; Lu, Jin, & Li, 2019). This phase change represents a pivotal hydrodynamic event, the prediction of which is essential for forecasting subsequent flow regimes—a principle well established in multiphase flow literature (Li, Zhu, Zhang, & Luo, 2023; Michaelides, Crowe, & Schwarzkopf, 2016; Sommerfeld, 2017; Zhu et al., 2022). The accurate determination of this initial flash depth is therefore paramount, as it governs fundamental well performance metrics, including wellhead steam quality, the pressure gradient, flow stability, and the potential for scaling or corrosion (Cheruiyot, 2019; Jacob & Favour, 2018). Consequently, reliably identifying the onset of the two-phase flow region is a prerequisite for optimizing field operations and informing critical decisions related to chemical inhibitor injection, orifice valve sizing, artificial lift implementation, and surface separator design (Alsubaih, Sepehrnoori, Delshad, & Alsaedi, 2025).

Wellbore modeling for geothermal systems is a mature field; conventional methodologies predominantly treat the working fluid as a pure water or steam-water binary system (Björnsson, 2010). This simplification persists despite the well-documented prevalence of significant concentrations of non-condensable gases (NCGs)—notably carbon dioxide ($CO_2$)—in geothermal brines, the thermodynamic influence of which is substantial. The solubility of $CO_2$ and its subsequent exsolution alter fundamental fluid properties—including density, specific enthalpy, and the pressure-temperature saturation curve—thereby displacing the first flash point to greater depths (Arancibia & Björnsson, 2020). Furthermore, the degassing of $CO_2$ modifies interphase mass transfer dynamics, perturbs developing two-phase flow regimes, and consequently distorts the wellbore's pressure profile (Gruber, 2016; Nassabeh, Iglauer, Keshavarz, & You, 2023; Yang et al., 2020). The omission of these $CO_2$-driven effects in classical models can therefore introduce significant predictive inaccuracies in flashing behavior and well deliverability—a concern particularly acute in high-enthalpy reservoirs where NCG concentrations frequently range from 5 to 20 wt% (Méndez & García, 2022).

Previous research on geothermal well modeling has generally focused on simulations of the overall pressure–temperature (P–T) evolution and wellhead conditions, with the starting point of flashing treated only as an implicit result when the fluid trajectory enters the saturation curve, rather than as an explicitly calculated primary variable. Various mechanistic models have integrated friction loss, conductive heat transfer, well geometry and formulation, as well as single- and two-phase flow formulations; meanwhile, thermodynamic studies have elucidated the criteria for transitioning to two-phase flow. Nevertheless, the effects of non-condensable gases such as $CO_2$ are generally modeled statically or at reservoir scale and are calculated only after flashing is assumed to occur.

Complexity is further increased in integrated THMC simulators, which, while comprehensive, make it difficult to explicitly trace the relationship between dynamic gas solubility, local heat transfer, and P–T trajectories along the well. Therefore, there is still a research gap in the form of the need for an efficient, depth-based numerical model that can explicitly predict the location of the first flash point, integrate pressure- and temperature-dependent $CO_2$ solubility based on Henry's law, and continue simulations consistently into a two-phase flow regime—given that flashing is affected nonlinearly by changes in the thermophysical properties of fluids, heat exchange with formations, and the presence of non-condensable gases.

This study aims to develop and apply a numerical model based on the Euler–Cauchy method to explicitly predict the depth of the initial flash point in the flow of geothermal fluids in the wellbore, taking into account the evolution of pressure–temperature, heat transfer with formations, and the dynamic influence of fluid thermophysical properties. The benefits of this study are to provide simple yet accurate and computationally efficient modeling tools to identify the initial location of flashing, improve understanding of the mechanism of the one-phase to two-phase transition in geothermal wells, and support well design planning, optimization of production operations, and mitigation of operational risks related to the uncertainty of flashing depth in the development of geothermal systems.

## METHOD

A one-dimensional, steady-state wellbore flow model is presented to explicitly determine the depth of the first flash point, with a particular focus on the thermodynamic role of dissolved $CO_2$. The model's methodology is based on a finite-difference, Euler–Cauchy numerical scheme for solving the coupled conservation equations.

### Governing Equations

The model is based on the following set of governing equations for a one-dimensional control volume, accounting for the presence of a non-condensable gas ($CO_2$) in the fluid mixture (Hasan & Kabir, 2002).

**a. Mass Conservation (Continuity Equation):**

The total mass flow rate is constant along the wellbore.

$$\frac{d\dot{m}}{dz} = 0 \text{ or } \dot{m} = \rho u A = \text{constant} \tag{1}$$

where $\dot{m}$ is the mass flow rate (kg/s), $\rho$ is the mixture density (kg/m³), $u$ is the velocity (m/s), $A$ is the cross-sectional area of the wellbore (m²), and $z$ is the depth (m).

**b. Momentum Conservation (Pressure Gradient Equation):**

The total pressure gradient is a sum of the static head, friction, and acceleration for a vertical well with axial coordinate $z$ (positive upward), the differential momentum equation is (Hasan & Kabir, 2010; Economides et al., 2013):

$$\frac{dP}{dz} = -\rho g - \frac{f\rho v^2}{2D} - \frac{d}{dz}(\rho v^2) \tag{2}$$

**Euler–Cauchy discretization**:

$$P_{i+1} = P_i + \Delta z[-\rho_i g - \frac{f_i\rho_i v_i^2}{2D} - \frac{\rho_{i+1}v_{i+1}^2 - \rho_i v_i^2}{\Delta z}] \tag{3}$$

Hasan & Kabir (2010); Economides et al. (2013); Ouyang et al. (1997); Mukherjee & Brill (1985).

**c. Energy Conservation (Thermal Energy Equation):**

The change in fluid enthalpy is governed by the work of expansion and heat transfer with the surrounding formation, following the foundational approach of Ramey (1962).

$$\frac{dh}{dz} = -g\cos\,\theta + \frac{q}{dz} \tag{4}$$

where $h$ is the specific enthalpy of the fluid mixture (J/kg). The heat transfer rate per unit depth, $q/dz$ (W/m), is modeled using Ramey's (1962) approach, which expresses it as a function of the fluid temperature, geothermal gradient, and overall heat transfer coefficient.

The energy balance including kinetic effects and wellbore heat loss is (Ramey, 1962; Hasan & Kabir, 2002):

$$\frac{dT}{dz} = \frac{q'(z) - v\frac{dP}{dz}}{\rho v C_p} \quad (5)$$

**Euler–Cauchy discretization**:

$$T_{i+1} = T_i + \Delta z \frac{q'(z_i) - v_i(\frac{P_{i+1} - P_i}{\Delta z})}{\rho_i v_i C_{p,i}} \quad (6)$$

Ramey (1962); Hasan & Kabir (2002); Pruess (1985); O'Sullivan et al. (2001).

**Thermodynamic Framework with $CO_2$ Solubility**

A critical component of this model is the integration of a $CO_2$-$H_2O$ thermodynamic framework, building on the work of studies like Saraçoğlu et al. (2021).

- **Solubility:** The mass of dissolved $CO_2$ in the liquid phase is calculated using Henry's Law, expressed in terms of mass fraction $x_{CO_2,l}$:

$$x_{CO_2,l} = \frac{K_H(T)}{P} \cdot M_{CO_2} \quad (7)$$

  where $K_H(T)$ is the temperature-dependent Henry's constant (Pa), and $M_{CO_2}$ is the molar mass of $CO_2$ (kg/mol).
- **Saturation Pressure:** The presence of dissolved $CO_2$ elevates the bubble-point (saturation) pressure of the mixture, a key effect highlighted by Arancibia & Björnsson (2020). The model calculates this modified saturation pressure $P_{sat,mix}$ iteratively, ensuring it is higher than the saturation pressure of pure water $P_{sat,H_2O}(T)$ at a given temperature.
- **Mixture Properties:** The thermophysical properties of the $CO_2$-$H_2O$ mixture (density $\rho_{mix}$, enthalpy $h_{mix}$, viscosity) are calculated as weighted functions of the component properties based on the local $CO_2$ mass fraction and phase state, using correlations established in the literature (e.g., Lei, 2022).

**Numerical Discretization: Euler–Cauchy Scheme**

The system of coupled ordinary differential equations is solved using an explicit Euler–Cauchy (depth-marching) finite-difference method, a technique effectively employed in wellbore simulation by Acuña (2013). The wellbore is discretized into small segments of length $\Delta z$, and the solution is marched upward from a known bottom-hole condition.

For a given depth step $i$, the state at the next step $i + 1$ is calculated explicitly. The general form for a generic variable $\phi$ (which can be $P$, $T$, or $h$) is:

$$\phi_{i+1} = \phi_i + (\frac{d\phi}{dz})_i \cdot \Delta z \quad (8)$$ Type equation here.

The application to each governing equation is as follows:

1. **Pressure Update:**

$$P_{i+1} = P_i + [(\rho g \cos\ \theta)_i + (\frac{f\rho u^2}{2D})_i + (\frac{d}{dz}(\rho u^2))_i]\Delta z \quad (9)$$

2. **Temperature and Phase State Update:**
   The new temperature $T_{i+1}$ is determined from the updated pressure $P_{i+1}$ and enthalpy $h_{i+1}$ using the $CO_2$-$H_2O$ thermodynamic property routines.
   - The model checks if the fluid is in a single-phase or two-phase state by comparing the mixture's saturation pressure $P_{sat,mix}(T_{i+1})$ with the local pressure $P_{i+1}$.
   - Flash Point Detection**:** The first flash point is explicitly identified as the depth where $P_{i+1} \leq P_{sat,mix}(T_{i+1})$ for the first time during the upward march, addressing a key gap in models that infer this point implicitly (Sarmiento & Björnsson, 2020).

**Solution Algorithm**

The simulation proceeds according to the following iterative algorithm for each depth step:

1. Start at the bottom-hole (node $i = 0$) with known initial conditions $P_0, T_0, \dot{m}$, and $CO_2$ mass fraction.
2. Calculate the pressure, and temperature gradients at the current node $i$.
3. March Upward: Use the Euler–Cauchy scheme to compute the new state $(P, T)_{i+1}$ at the next node.
4. Evaluate Thermodynamics: Update the $CO_2$ solubility and calculate the mixture saturation pressure $P_{sat,mix}$ at $T_{i+1}$.
5. Check for Flashing: If $P_{i+1} \leq P_{sat,mix}$, record the depth as the First Flash Point and switch the fluid property routines to a two-phase, gas-liquid mixture model for all subsequent steps.

This methodology provides a robust, transparent, and computationally efficient framework for explicitly tracking the thermodynamic state of a $CO_2$-rich geothermal fluid and pinpointing the exact depth where two-phase flow initiates, filling a critical gap between large-scale THMC models and simplified wellbore simulators (Wapperom et al., 2022). The study process is captured on Fig.1.

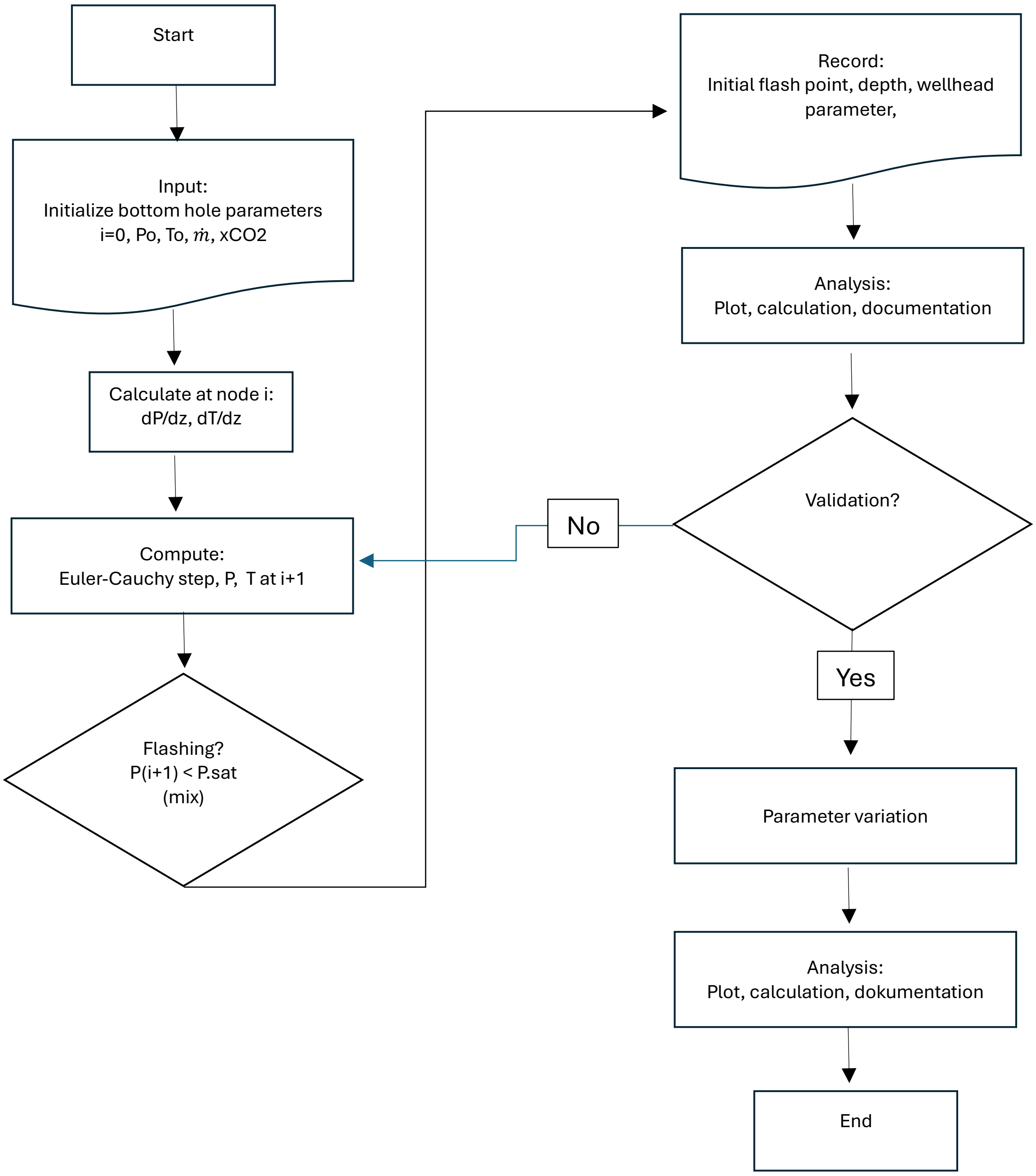


**Fig.1** Research Flowchart

The simulation follows a systematic, iterative computational procedure to model fluid flow and determine the first flash point in a geothermal wellbore. The workflow, illustrated in Figure 1, can be formally described as follows:

The process is initialized by defining the bottom-hole conditions at node i=0, including initial pressure ($P_0$), temperature ($T_0$), mass flow rate ($\dot{m}$), and the $CO_2$ mass fraction ($xCO_2$). The core of the algorithm is a depth-marching loop. For each node i, the local gradients of pressure, and temperature with respect to depth (dP/dz, dT/dz) are computed. These gradients are then used in an explicit Euler-Cauchy numerical step to calculate the corresponding state variables (P, T) at the subsequent upstream node i+1.

A critical thermodynamic check is performed at this new node to determine if the fluid undergoes flashing. This is achieved by comparing the local pressure P(i+1) against the $CO_2$-$H_2O$ mixture's saturation pressure P_sat (mix). If the condition P(i+1) ≤ P_sat (mix) is met, the depth is recorded as the first flash point, and key wellhead parameters are subsequently calculated based on the continued simulation to the surface.

Following the simulation's completion, the results—including the flash point depth, pressure, and temperature profiles—are subjected to a validation step against established analytical solutions or field data. If the validation is successful, the process moves to the analysis phase, which involves plotting the results, performing quantitative calculations, and documenting the findings. If the model fails validation, a parameter variation study is initiated, where input parameters are systematically adjusted, and the simulation is rerun until a satisfactory agreement is achieved. The final stage encompasses a comprehensive analysis of the validated results, including data visualization and the preparation of technical documentation.

**Table 1. Data initialization**

| Parameter | Value |
|---|---|
| Bottom Pressure, bar | 80 |
| Bottom Temperature, °C | 260 |
| Mass Flow Rate, kg/s | 50 |
| Wellbore Diameter, m | 0.2 |
| Well Depth, m | 1500 |

The initialization variables presented in Table 1 constitute the essential boundary conditions for resolving the interdependent mass, momentum, and energy equations that describe fluid behavior within a geothermal wellbore. The choice of these inputs directly affects the model's capacity to represent phase changes, thermal gradients, and the overall hydrodynamic evolution as the fluid ascends the well.

The specified bottom-hole pressure of 80 bar reflects the natural reservoir driving force while also establishing the initial thermodynamic state of the produced fluid. Under such pressure, the geothermal fluid generally remains in a compressed liquid phase. As the fluid flows upward and experiences pressure reductions due to hydrostatic unloading and frictional resistance, the solution tracks the fluid's progression toward the saturation boundary. This enables determination of the initial flash point, the depth at which vapor formation begins and two-phase flow emerges. Accurate representation of reservoir pressure is therefore critical, as errors may lead to unrealistically early or late flashing, a common numerical challenge in geothermal well modelling.

Likewise, the bottom-hole temperature of 260 °C sets the thermophysical reference point for calculating key properties such as density, viscosity, specific heat, and thermal conductivity. Even moderate variations in this temperature can shift the predicted saturation line, where higher temperatures generally raise enthalpy and cause flashing to occur at shallower depths. In addition, the temperature contrast between the fluid and the surrounding formation governs wellbore heat loss, influencing the energy balance throughout the ascent. Within an Euler–Cauchy integration scheme, this temperature acts as the initial state for iterative updates, making its precision essential for maintaining numerical robustness.

The mass flow rate of 50 kg/s determines the momentum of the rising fluid and regulates the interplay between inertial forces and frictional dissipation. Increased flow rates enhance turbulence, reduce thermal residence time, and can postpone flashing by sustaining higher downhole pressures. In contrast, smaller flow rates allow more heat to dissipate to the formation, which may cause the flashing event to occur deeper in the well. Practically, this parameter is closely tied to production optimization, pump sizing, and sustainable resource utilization.

The wellbore diameter of 0.20 m characterizes the flow passage and influences several hydraulic and thermal phenomena, including: a) The cross-sectional area, which determines velocity for a specified mass flow rate. b) The friction factor, dependent on both diameter and flow regime, c) The wall heat-transfer coefficient, which governs thermal exchange with the surrounding rock.

A reduced diameter typically increases frictional pressure losses and fluid velocity, potentially promoting earlier transition to two-phase flow. Conversely, a larger diameter may reduce pressure gradients but increase radial heat dissipation. The well depth of 1500 m defines the physical domain for numerical integration using the Euler–Cauchy method. The vertical discretization interval ($\Delta z$) strongly influences the resolution of temperature and pressure profiles, particularly near the flashing zone where gradients intensify. A 1500 m depth is representative of many geothermal production wells and provides a suitable framework for comparing model outputs with field observations and established research. Each parameter in Table 1 contributes a distinct role within the Euler–Cauchy computational procedure as shown in Table 2.

**Table 2. Role of Initial Parameters**

| Parameter | Computational Function in Euler–Cauchy Scheme |
|---|---|
| Bottom Pressure | Sets the initial momentum conditions and governs the detection of flashing onset. |
| Bottom Temperature | Establishes the initial thermal state for energy conservation calculations. |
| Mass Flow Rate | Controls velocity, frictional losses, and convective heat transport. |
| Wellbore Diameter | Influences hydraulic area, Reynolds number, and associated friction factors. |
| Well Depth | Defines the vertical range over which iterative updates are applied. |

At every incremental depth step, the model updates the governing equations to determine: a) The pressure gradient (dp/dz), derived from the momentum balance. b) The temperature gradient (dT/dz), obtained from the energy equation. c) The vapor fraction and slip conditions once flashing occurs. c) $CO_2$ dissolution or exsolution effects when relevant, modelled via Henry's law or appropriate equations of state.

## RESULT AND DISCUSSION

### Pressure–Depth Profiles Under Varying $CO_2$ Concentrations

Figure 2 presents the simulated pressure–depth profiles for geothermal wellbore flow under different dissolved $CO_2$ concentrations (0–1.0%). The curves represent the evolving fluid pressure from the wellhead to the reservoir depth of 1500 m, while the circular markers denote the predicted initial flash point, defined as the depth at which the fluid first intersects the saturation pressure curve and begins transitioning into two-phase flow.

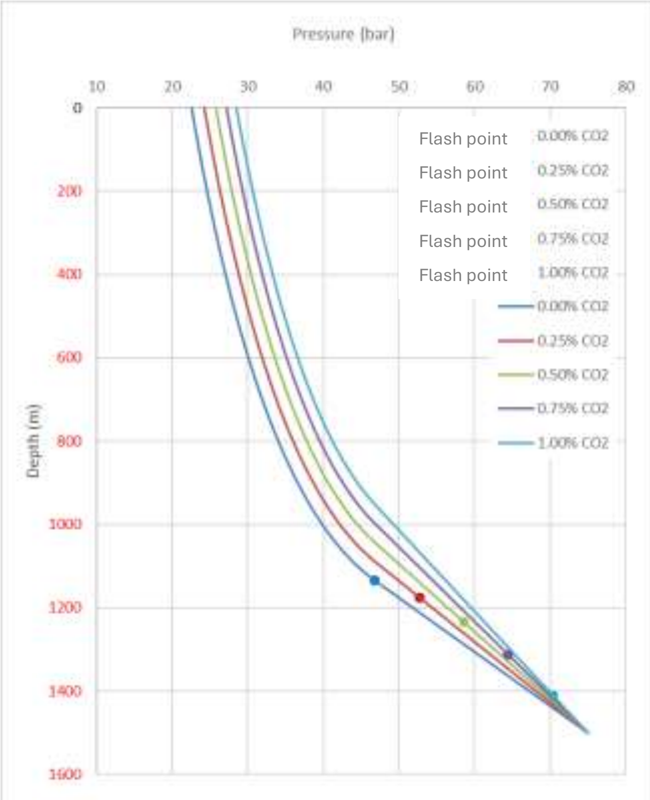


**Fig.2** Flash point and pressure profile with various CO2

The pressure–depth trajectories show a systematic shift associated with increasing $CO_2$ content. As the dissolved $CO_2$ fraction rises from 0% to 1.0%, the pressure curves become progressively shallower and exhibit slightly reduced hydraulic gradients. This behaviour stems from two principal mechanisms:

1. Reduction in Liquid Density

Dissolved $CO_2$ lowers the density of the geothermal brine due to its lower molecular weight and non-ideal mixing effects. A decrease in fluid density reduces the hydrostatic pressure component, resulting in a slower increase in pressure with depth. Prior studies have documented that $CO_2$–$H_2O$ mixtures can significantly alter density behaviour, especially at reservoir-scale pressures and temperatures (Spycher & Pruess, 2005; Duan & Sun, 2003).

2. Enhanced Compressibility Effects

$CO_2$-rich geothermal fluids exhibit greater compressibility than pure water, influencing the pressure gradient during upflow and amplifying deviations from the single-component fluid case. This phenomenon has been emphasized in geothermal thermodynamic modelling literature, where multicomponent systems often deviate from classical hydrostatic predictions (O'Sullivan et al., 2001). These combined effects cause the pressure profiles to diverge, with higher $CO_2$ contents shifting the curves to the right (toward higher pressure at a given depth) in the upper wellbore and delaying depressurization during ascent.

The circular markers on each curve represent the initial flash point, where fluid pressure equals the saturation pressure corresponding to the local temperature. This intersection marks the transition from single-phase liquid flow to two-phase liquid–vapor flow. The results clearly show that, the higher $CO_2$ concentrations produce deeper flash points. For example, the pure-water case (0% $CO_2$) flashes at 1134.00 m, while the 1.0% $CO_2$ case flashes at 1409.50 m. This trend aligns with established thermodynamic principles:

1. $CO_2$ Dissolution Raises the Saturation Pressure

The presence of $CO_2$ increases the mixture's vapor pressure through solubility interactions and shifts the liquid–vapor equilibrium curve upward. As a result, the fluid must depressurize further (i.e., ascend higher) before vaporization can initiate. This effect is well documented in geothermal phase-equilibrium analyses (Giggenbach, 1980; Spycher & Pruess, 2010).

2. Delayed Flashing Due to Modified Thermophysical Properties

$CO_2$-rich fluids require larger pressure drops to reach saturation because their thermophysical properties—particularly density, compressibility, and heat capacity—differ from pure water. Studies of $CO_2$–water mixtures in geothermal and magmatic systems have repeatedly shown delayed onset of boiling in $CO_2$-containing fluids (Kharaka et al., 2006; Aradóttir et al., 2014).

The shift of the flash point with $CO_2$ concentration is significant for geothermal well design: a) A deeper flash point increases the length of the single-phase region, reducing two-phase flow–related instabilities such as slugging or high frictional losses. b) However, delayed flashing may reduce wellhead enthalpy, resulting in lower steam fraction at the surface. c) $CO_2$ must therefore be accounted for in geothermal well performance forecasting, especially in volcanic geothermal systems where $CO_2$ content is naturally elevated.

These outcomes agree with field evidence from $CO_2$-rich geothermal reservoirs—such as those in Iceland and New Zealand—where dissolved gases are known to significantly modify wellbore thermal conditions and production performance (Gudmundsson & Björnsson, 1993; Bloomfield & Bannister, 2001).

**Temperature – Depth Profiles due to Flash Point**

Figure 3 illustrates the temperature–depth behavior of geothermal fluid for various dissolved $CO_2$ concentrations (0–1.0%) and highlights the evolution of temperature after the onset of flashing. The temperature curves reveal a distinct change in gradient following the initial flash point, indicated by the circular markers. This inflection reflects the transition from single-phase liquid flow to a two-phase liquid–vapor mixture, which fundamentally alters the system's thermodynamic and heat-transfer characteristics.

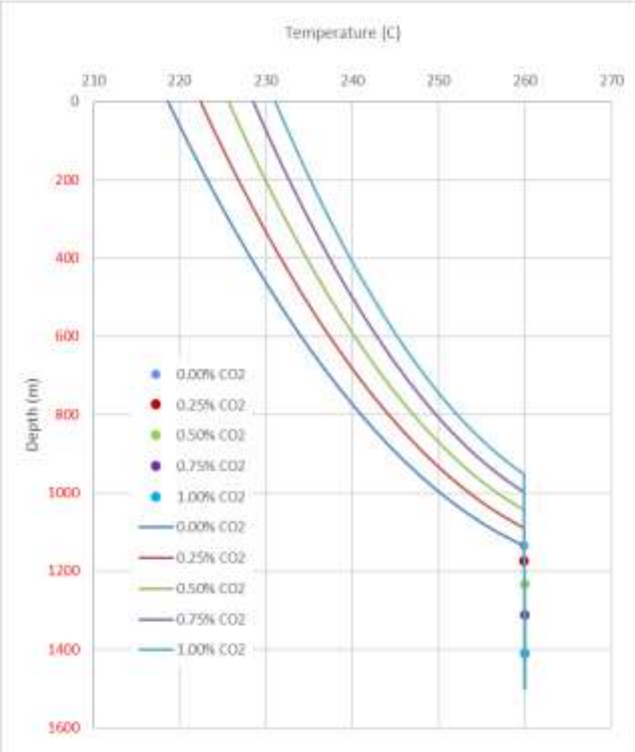


**Fig.3** Flash point and temperature profile

Once the fluid reaches the saturation envelope and boiling initiates, the temperature profile exhibits a reduced rate of decline with decreasing depth. This behavior is attributable to the latent heat effect, where a portion of the fluid's thermal energy is consumed to generate vapor rather than contributing solely to sensible heat loss. Consequently, the temperature becomes strongly constrained by the saturation temperature corresponding to the local pressure, and the fluid tends to follow a near-isothermal or weakly decreasing temperature trend during subsequent ascent. This thermodynamic phenomenon is well established in geothermal wellbore studies, where the onset of two-phase flow is accompanied by a characteristic flattening of the temperature gradient (Lipschultz & Ramey, 1966; Björnsson, 1978). The dominant heat–mass coupling in this region means that temperature becomes less sensitive to conductive heat loss to the formation and more dependent on phase equilibrium conditions.

The results show that increasing $CO_2$ concentration systematically shifts the post-flash temperature profiles downward, indicating flashing at greater depths and lower temperatures. Two primary mechanisms explain this behavior: $CO_2$ dissolution decreases the water phase's activity, thereby altering the saturation curve. This generally leads to a lower saturation temperature at a given pressure, consistent with the vapor–liquid equilibrium behavior of $CO_2$–$H_2O$ mixtures (Spycher & Pruess, 2010; Duan & Sun, 2003). Consequently, $CO_2$-rich fluids can remain in single-phase liquid conditions to greater depths, delaying the onset of stable two-phase conditions.

The addition of $CO_2$ increases the mixture's effective heat capacity and compressibility, allowing the fluid to retain thermal energy more efficiently during ascent. Prior geothermal studies have reported that gas-rich geothermal fluids display modified thermal gradients due to these compositional effects (Aradóttir et al., 2014; Kharaka et al., 2006). Fluids with higher $CO_2$ content exhibit lower temperatures at the flash point and maintain higher sensible heat retention afterward, producing the stratified temperature behavior evident in the figure.

**Pressure Gradient – Depth Profiles**

How pressure gradients evolve with depth for varying $CO_2$ fractions. A marked shift occurs after the flash point, indicated by the circular symbols. Above this transition, the gradient decreases smoothly with depth, whereas entry into the two-phase region produces a distinctly different gradient behavior driven by multiphase flow effects.

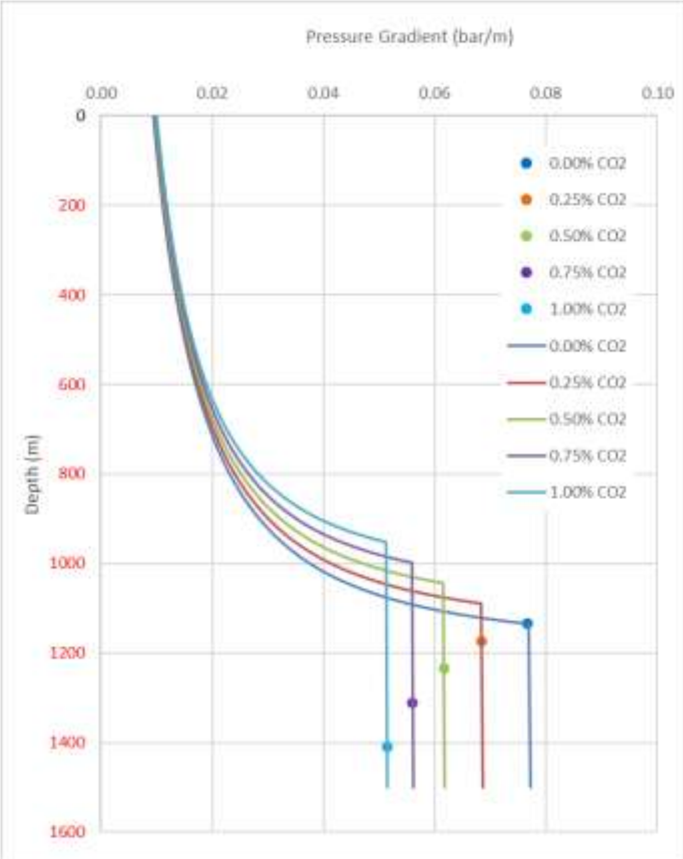


**Fig.4** Pressure gradient profile

After the flash point, the pressure gradients increase sharply, reflecting the transition from a single-phase liquid to a liquid–vapor mixture. This change is governed by two principal mechanisms:

1. Increase in Frictional Pressure Losses
   Two-phase flow introduces higher friction factors and slip effects, leading to elevated momentum losses compared with single-phase liquid flow. The presence of vapor increases mixture velocity and turbulence, thereby amplifying pressure dissipation (Hasan & Kabir, 1990; Wang et al., 1997).
2. Reduction in Effective Mixture Density
   Vapor generation significantly reduces the mixture density, intensifying the hydrostatic contribution to the pressure gradient. This effect is consistent with classical geothermal

wellbore analyses, where boiling causes abrupt increases in dp/dz (Ramey, 1962; Björnsson, 1978).

The position and magnitude of the pressure-gradient increase are strongly influenced by dissolved $CO_2$ content. Higher $CO_2$ concentrations delay the flash point to deeper depths, causing the rapid increase in dp/dz to occur farther down the wellbore. This trend reflects established $CO_2$–$H_2O$ thermodynamic behavior:

$CO_2$ lowers saturation temperature, shifting the boiling onset deeper in the well (Spycher & Pruess, 2010; Duan & Sun, 2003).

$CO_2$-rich fluids exhibit modified viscosities and compressibilities, which influence phase-slip behavior and frictional pressure losses during boiling (Aradóttir et al., 2014; Kharaka et al., 2006).

Understanding the pressure-gradient response after flashing is critical for predicting two-phase flow stability, estimating wellhead pressure and steam quality, and optimizing wellbore design to minimize excessive frictional losses.

**Temperature-Gradient Behavior**

Figure 5 presents the vertical evolution of temperature gradients for geothermal wellbore flow under varying dissolved $CO_2$ contents. The circular markers denote the initial flash point, after which all curves transition into a distinct regime governed by two-phase thermodynamics. Prior to flashing, the temperature gradient decreases with depth due to diminishing heat loss to the surrounding formation and changes in fluid thermophysical properties. Once boiling begins, however, the temperature gradients exhibit markedly different behavior.

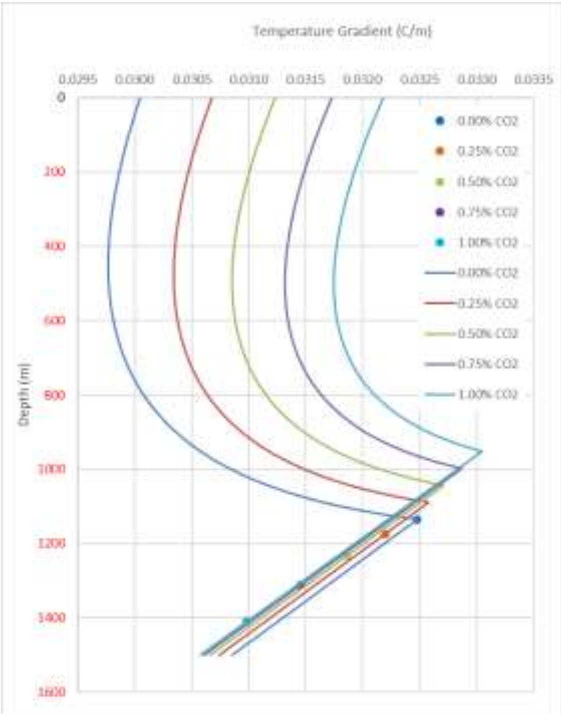


**Fig.5** Temperature gradient profile

After the fluid reaches the saturation envelope and vapor generation commences, the temperature gradient becomes significantly flatter. This arises because, in the two-phase region, much of the thermal energy is expended as latent heat of vaporization, leaving less energy available for sensible temperature change. As a result, the fluid temperature remains near saturation and declines only minimally with depth (Ramey, 1962; Lipschultz & Ramey, 1966). This phenomenon is characteristic of two-phase geothermal wellbore flow, where the temperature profile becomes strongly pressure-dependent rather than heat-transfer dominated.

In addition, the onset of boiling substantially alters the mixture's effective heat capacity. The increased specific enthalpy associated with vapor fractions contributes to a more uniform thermal gradient, consistent with two-phase heat-transfer theory and geothermal production well observations (Björnsson, 1978; O'Sullivan et al., 2001).

The plotted results show that increasing $CO_2$ content systematically shifts the two-phase temperature-gradient curves deeper into the wellbore. This behavior reflects the known influence of dissolved $CO_2$ on phase equilibrium. $CO_2$ reduces the saturation temperature at a given pressure, delaying the onset of boiling and shifting the two-phase region downward (Spycher & Pruess, 2010; Duan & Sun, 2003). $CO_2$ modifies the mixture heat capacity and entropy, resulting in a slightly steeper temperature gradient once two-phase flow develops (Aradóttir et al., 2014; Kharaka et al., 2006).

The sharp contrast between pre-flash and post-flash behavior in geothermal wellbore profiles arises from a fundamental change in fluid thermodynamic state—from single-phase liquid to two-phase liquid–vapor. This transition triggers major changes in density, viscosity, enthalpy, heat transfer, and momentum balance that alter how temperature and pressure evolve with depth.

The pronounced difference between the pre-flash and post-flash gradients in the geothermal wellbore arises from a fundamental shift in the thermodynamic regime of the flowing fluid. Prior to flashing, the fluid remains in a single-phase liquid state, and its temperature and pressure gradients are governed primarily by sensible heat loss to the surrounding formation, hydrostatic loading, and frictional resistance. Under these conditions, thermophysical properties vary smoothly with depth, producing relatively uniform and predictable gradient profiles.

When the fluid reaches saturation and vapor nucleation begins, the system transitions into a two-phase liquid–vapor region. This change introduces strong nonlinearities in density, viscosity, and enthalpy, which significantly alter both the momentum and energy balances. In the two-phase regime, a substantial fraction of the thermal energy is consumed as latent heat of vaporization, limiting the rate of sensible temperature decline and causing the temperature gradient to shift toward a saturation-controlled behavior. At the same time, the rapid reduction in mixture density and increased slip between phases lead to elevated frictional pressure losses, resulting in a marked increase in the pressure gradient.

As documented in geothermal wellbore theory, this transition produces a characteristic discontinuity or inflection in both pressure and temperature profiles, reflecting the dominance of phase-change processes over conventional hydrothermal mechanisms (Ramey, 1962; Björnsson, 1978; Hasan & Kabir, 1990; Spycher & Pruess, 2010). Therefore, the significant difference in patterns before and after the flash point is a direct consequence of the onset of two-phase flow and the associated shifts in thermodynamic and hydrodynamic behavior.

**Pressure–Temperature Behavior**

Presents the pressure–temperature (P–T) relationship at the predicted flash points for varying dissolved $CO_2$ concentrations. The results demonstrate that increasing $CO_2$ content systematically lowers the saturation temperature corresponding to a given pressure, causing the flash point to occur at progressively lower temperatures as $CO_2$ concentration rises. This trend is consistent with the thermodynamic behavior of $CO_2$–$H_2O$ mixtures, in which dissolved $CO_2$ reduces water activity and depresses the saturation temperature through non-ideal phase interactions (Duan & Sun, 2003; Spycher & Pruess, 2010).

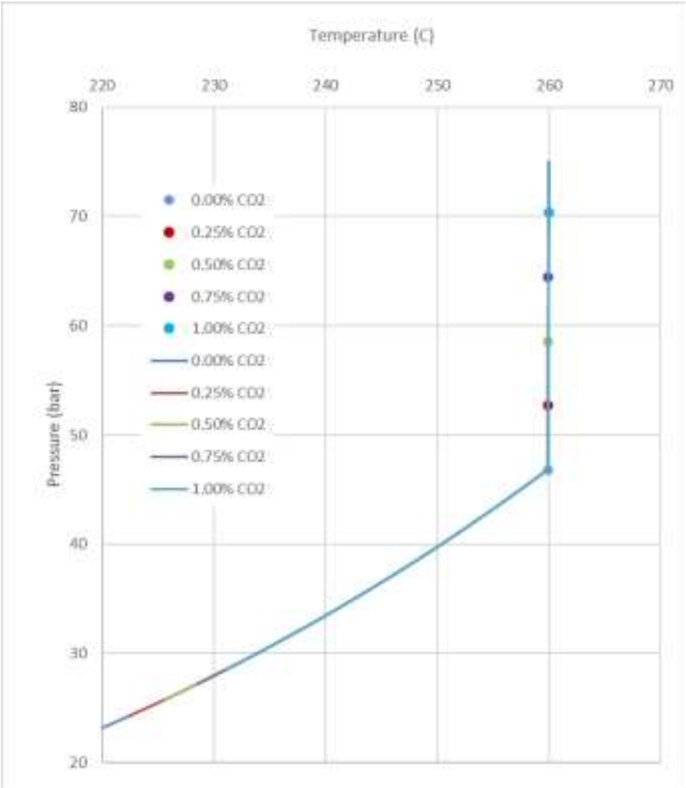


**Fig.6** Pressure and temperature profile

The vertical alignment of pressures across different $CO_2$ fractions indicates that the flash points occur along similar pressure levels determined by the wellbore pressure profile; however, the associated temperatures differ due to compositional effects. Such behavior has been documented in gas-rich geothermal systems, where dissolved $CO_2$ modifies phase equilibria, shifts boiling conditions, and alters the thermal state at the onset of two-phase flow (Aradóttir et al., 2014; Kharaka et al., 2006). Overall, the figure confirms that $CO_2$ plays a significant role in controlling geothermal flashing behavior by adjusting the P–T conditions required for vaporization.

**CONCLUSION**

The numerical evaluation of geothermal wellbore flow under varying dissolved $CO_2$ concentrations reveals that compositional effects decisively shape the thermodynamic and hydraulic behavior of ascending fluids, with increasing $CO_2$ content systematically delaying flashing onset and shifting the initial flash point to deeper depths due to saturation temperature depression. Pressure–depth and temperature–depth profiles, along with gradient analyses, show smooth single-phase evolution governed by hydrostatic, frictional, and heat-loss effects transitioning abruptly post-flash into two-phase regimes marked by density changes, enhanced friction, phase slip, and latent-heat constraints—producing characteristic inflections. P–T mapping further confirms $CO_2$ as a key thermodynamic modifier that lowers the saturation curve without major pressure shifts, affirming its critical role in accurate wellbore modeling consistent with prior geothermal studies. For future research, integrating real-time $CO_2$ exsolution dynamics with machine learning-based sensitivity analyses could enhance predictive fidelity across diverse reservoir compositions and operational scales.

## REFERENCES

Alsubaih, A., Sepehrnoori, K., Delshad, M., & Alsaedi, A. (2025). A comprehensive review of well integrity challenges and digital twin applications across conventional, unconventional, and storage wells. *Energies*.

Arancibia, M., & Björnsson, G. (2020). Modeling the effects of non-condensable gases in geothermal wells. *Geothermics, 88*, 101879. https://doi.org/10.1016/j.geothermics.2020.101879

Cheruiyot, B. K. (2019). *Load optimization by steam and blade washing in a flash type power plant: A case study of Olkaria II geothermal power plant* (Tesis).

Gruber, C. (2016). *Two-phase flow investigations of gas-kick scenarios: Application of computational fluid dynamics to kick analysis in wellbores* (Disertasi).

Guo, J., Xiong, W., Hu, Q. Y., Tian, Y., He, X., Zhang, L. H., Zhao, Y. L., & Zhang, T. (2022). Stability analysis and two-phase flash calculation for confined fluids in nanopores using a novel phase equilibrium calculation framework. *Industrial & Engineering Chemistry Research, 61*(32), 12032–12046. https://doi.org/10.1021/acs.iecr.2c01645

Ibrahim, A. T. (2021). A review of mathematical modelling approaches to tackling wellbore instability in shale formations. *Journal of Natural Gas Science and Engineering, 91*, 103957. https://doi.org/10.1016/j.jngse.2021.103957

Jacob, N. C. G., & Orisa, F. E. (2018). An integrated well-reservoir steam injection modelling for steam injection optimization. *International Journal of Advanced Engineering Research and Science, 5*(6), 178–186.

Lei, W. (2022). Thermodynamic behavior of $CO_2$–water mixtures in geothermal applications. *Energy, 254*, 124328. https://doi.org/10.1016/j.energy.2022.124328

Li, S. J., Zhu, L., Zhang, X. B., & Luo, Z.-H. (2023). Recent advances in CFD simulations of multiphase flow processes with phase change. *Industrial & Engineering Chemistry Research, 62*(6), 2143–2167. https://doi.org/10.1021/acs.iecr.2c04064

Liu, Q., Xiao, B., Zhuang, G., Li, Y., & Li, Q. (2025). Instability mechanisms and wellbore-stabilizing drilling fluids for marine gas hydrate reservoirs: A review. *Energies*.

Lu, C., Jin, Z., & Li, H. A. (2019). A two-phase flash algorithm with the consideration of capillary pressure at specified mole numbers, volume and temperature. *Fluid Phase Equilibria, 483*, 28–37. https://doi.org/10.1016/j.fluid.2018.11.012

Méndez, C., & García, C. (2022). Influence of non-condensable gases on geothermal well deliverability. *Renewable & Sustainable Energy Reviews, 158*, 112097. https://doi.org/10.1016/j.rser.2022.112097

Michaelides, E. E., Crowe, C. T., & Schwarzkopf, J. D. (2016). *Fundamentals of multiphase flow*. CRC Press.

Nassabeh, M., Iglauer, S., Keshavarz, A., & You, Z. (2023). Advancements, challenges, and perspectives of flue gas injection in subsurface formations: A comprehensive review. *Energy & Fuels, 37*(6), 4023–4052. https://doi.org/10.1021/acs.energyfuels.2c04131

Saraçoğlu, H., Erol, S., & Korkmaz, S. (2021). Solubility and thermodynamic behavior of $CO_2$ in geothermal brines. *Journal of Petroleum Science and Engineering, 205*, 108905. https://doi.org/10.1016/j.petrol.2021.108905

Sarmiento, Z. F., & Björnsson, G. (2020). Thermodynamic criteria for flashing in geothermal wells. Dalam *Proceedings of the World Geothermal Congress 2020*. Reykjavik, Iceland.

Sommerfeld, M. (2017). *Numerical methods for dispersed multiphase flows*. Springer.

Su, X., & Wang, H. (2023). Multiphase wellbore modeling incorporating non-condensable gases. *Journal of Petroleum Science and Engineering, 220*, 111194. https://doi.org/10.1016/j.petrol.2022.111194

Wapperom, P., et al. (2022). Integrated THMC modeling of geothermal well performance. *Renewable Energy, 185*, 320–334. https://doi.org/10.1016/j.renene.2021.12.050

Yang, H., Li, J., Liu, G., Xing, J., Hailong, H., & Wang, C. (2020). The effect of interfacial mass transfer of slip-rising gas bubbles on two-phase flow in the vertical wellbore/pipeline. *International Journal of Heat and Mass Transfer, 151*, 119397. https://doi.org/10.1016/j.ijheatmasstransfer.2020.119397

Zhu, L., Chen, X., Ouyang, B., Yan, W., Lei, H., Chen, Z., & Luo, Z.-H. (2022). Review of machine learning for hydrodynamics, transport, and reactions in multiphase flows and reactors. *Industrial & Engineering Chemistry Research, 61*(1), 1–23. https://doi.org/10.1021/acs.iecr.1c04348